Nanoscale

Accepted Manuscript

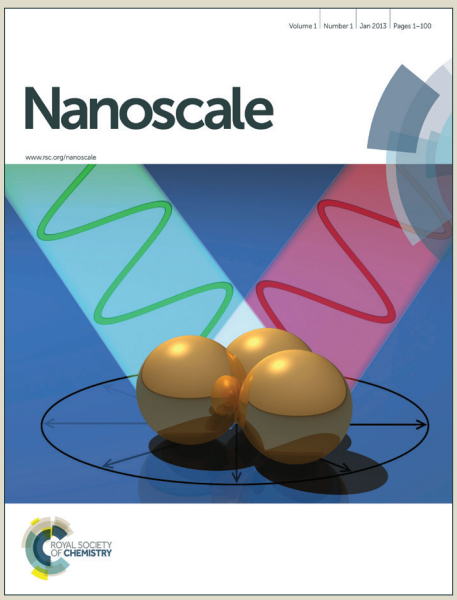

ROYAL SOCIETY OF CHEMISTRY

www.rsc.org/nanoscale

Journal Name

RSCPublishing

ARTICLE

Imaging of Drug Loading Distributions in Individual Microsphere of Calcium Silicate Hydrate - An X-ray Spectromicroscopic Study†

Cite this: DOI: 10.1039/xoxxoooooox

Received ooth January 2012,
Accepted ooth January 2012

DOI: 10.1039/xoxxoooooox

www.rsc.org/

Xiaoxuan Guo, ‡[a] Zhiqiang Wang, ‡[a] Jin Wu,[b] Jian Wang,[c] Ying-Jie Zhu*[b] and Tsun-Kong Sham*[a]

Imaging is one of the most direct and ideal ways to track drug loading distributions in drug carriers on the molecular level, which will facilitate the optimization of drug carrier and drug loading capacities. Herein, we report the mapping of an individual mesoporous calcium silicate hydrate (CSH) microsphere before and after the loading of ibuprofen (IBU) and the interactions between drug carriers and drug molecules simultaneously by scanning transmission X-ray microscopy (STXM). Nanoscaled X-ray absorption near edge structure (XANES) spectroscopy clearly indicates that IBU is bonded to calcium and silicate sites via carboxylic acid groups. More importantly, STXM has been successfully used to determine the absolute thickness of IBU, revealing its distribution in the CSH microsphere.

Introduction

The Calcium silicate based materials are promising for applications in biomedical fields with the advantages of having excellent biocompatibility, biodegradability. [1-4] As a matter of fact, calcium silicate hydrate (CSH) can be applied in periodontal repair and bone augmentation because of their stimulatory effect on osteogenic differentiation of stem cells.[5] For clinical applications, drug incorporation using CSH drug carriers allows for not only the repair of bone defects, but also bone therapies, such as bone anti-infection, fracture consolidation and tumor treatment.[6] Insufficient drug dose, however, is one of the most common issues in drug delivery systems, thus it is important to ensure the successful incorporation of drug molecules, and to determine the drug loading capacities for the next step. Although there are many conventional methods, such as UV-Vis, thermogravimetric analysis etc., to measure the drug loading amount in the drug carriers, the integrity and distributions of drug molecules, which are essential to the drug delivery and further drug release, cannot be revealed based on the conventional techniques. Besides, the interactions between drug molecules and carriers also play a crucial role on drug loading capacities.[7, 8] To realize this goal, it is necessary to image the variations of the local chemical composition in an individual drug carrier before and after drug loading. However, very few techniques can provide this unique information.

Scanning transmission X-ray microscopy (STXM)[9, 10] records the X-ray absorption features at an absorption edge of an element in a chemical environment in the transmission mode using a nano size X-ray beam. It provides spectromicroscopy information; thus both chemical images and detailed absorption spectroscopic features in the near edge region of a single nanostructure can be revealed, especially good for the low Z elements (such as C, O and N). More importantly, STXM can also measure the absolute thickness of the specimen. It has been successfully applied to study the iron-based Fischer–Tropsch catalyst,[11] individual multi-walled carbon nanotube,[12] graphene,[13] single ZnS/ZnO nano-heterostructure[14] and individual hybrid TiO_2 particles,[15] by providing unique composition of nanomaterials without significant beam damage. X-ray absorption near edge structure (XANES) spectroscopy provides information about the structure and bonding intimately associated with the absorbing atom and the immediate surroundings of the absorbing atom.[16] It is very sensitive to the slight changes of surrounding environment of target atoms via the noticeable changes of spectral features (peak energy shift, peak intensity variations, and dis/appearance of new features, *etc.*).[17-19] As a matter of fact, STXM-XANES is also suitable for drug delivery study. For example, it is

desirable to know the integrity of drug molecules, bonding information and their distributions after loading processes. The normal area of beam on the samples is around mm^2; consequently, the information from the XANES spectra is an average of a large area which may contain impurities from the substrate, especially for the organic materials. The improvement of spatial resolution of STXM overcomes the shortcoming above and provides information of isolated or individual structures of nanomaterials. Here, for the first time we report the application of STXM combined with XANES in the chemical imaging of individual CSH mesoporous microsphere loaded with model drug ibuprofen (IBU). The electronic and chemical structure of selected sample regions of sub-micron dimension were obtained by spatially-resolved XANES at the C, O, Si K-edges and the Ca $L_{3,2}$-edge.

Experimental

Preparation of CSH mesoporous microspheres

CSH mesoporous microspheres formed by self-assembly of CSH nanosheets were prepared via a sonochemical method.[20] 5 mL of a 4 M NaOH aqueous solution and 2 mL of tetraethyl orthosilicate (TEOS) were added into 500 mL of 0.03 M $Ca(NO_3)_2$ aqueous solution under magnetic stirring at room temperature. The resulting mixture was ultrasonically irradiated for 1 hour under ambient conditions using a high-intensity ultrasonic probe with the power of 200 W (Ti-horn, 27 kHz, Hangzhou Success, China) immersed directly in the solution. The product was centrifuged (6000 rpm for 2 min) and washed with deionised water and absolute ethanol three times, respectively. Then, the powder was dried in air at 60 °C overnight.

IBU drug loading

The as-synthesized powder (1.0 g of CSH mesoporous microspheres) was added to a 50 mL IBU hexane solution (~40 mg mL^{-1}) in a flask at room temperature. The flask was immediately sealed to prevent hexane from evaporation, and the mixture was treated by ultrasound for 2 minutes. Then the flask was oscillated at a constant rate of 160 rpm at 37 °C for 24 hours. The product was separated by centrifugation (6000 rpm for 2 min), washed with hexane, and dried in air at 60 °C overnight.

Characterization

The IBU hexane solutions before and after the IBU loading were analyzed by UV-Vis absorption (Techcomp, UV2300) at the wavelength of 263 nm. Transmission electron microscopy (TEM) images were obtained at the Biotron, University of Western Ontario (Philips CM-10 TEM).

STXM measurement

STXM measurement was conducted at the Soft X-ray Spectromicroscopy (SM) beamline at the Canadian Light Source (CLS); SM beamline is equipped with a 25 nm outermost-zone zone plate (CXRO, Berkeley Lab). The diffraction-limited spatial resolution for this zone plate is 30 nm with a spectral resolution of 0.05 eV. Image sequence (stack) scans over a range of photon energies were acquired for the same sample region at the Ca $L_{3,2}$-edge, and Si, O and C K-edges, respectively. A few mg of the sample was dispersed in deionised water by brief sonication, and then deposited on a copper grid to allow it to dry in air before transferring into the STXM chamber. STXM data were analyzed using the aXis2000 software package, which allows for detailed interactive processing of the images and fitting the image stacks with the X-ray absorption spectra.

Results and discussion

The UV-Vis absorption spectra of the hexane solution containing IBU before and after IBU loading in CSH mesoporous microspheres are shown in Figure 1. One can see that the absorption spectra of IBU in hexane show the characteristic absorption peaks of IBU, e.g. the most intense feature at 263 nm, which are consistent with the literature.[21] After IBU loading, a significant decrease in the absorbance of IBU in hexane solution (red profile) indicates that the IBU drug molecules have been loaded into the drug carriers with a high drug loading capacity.

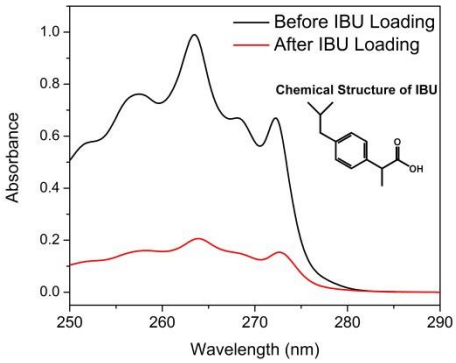

Fig. 1 UV-Vis absorption spectra of the IBU hexane solution diluted 50 times before and after the IBU loading in CSH mesoporous microspheres.

The morphology of the CSH mesoporous microspheres before and after IBU loading was characterized by TEM. As shown in Figure 2a, the sample before IBU loading is composed of mesoporous microspheres formed by self-assembly of nanosheets with diameters around 1 μm. The three-dimensional interconnected nanosheets lead to the formation of a large number of mesopores. It should be noted that the CSH mesoporous microspheres after IBU loading (see Figure 2b) show a similar morphology to that before IBU loading. Thus, TEM results clearly reveal that the morphology of CSH mesoporous microspheres remains intact after IBU loading, and it would be significant if we can identify the locations and distributions of IBU in the carriers.

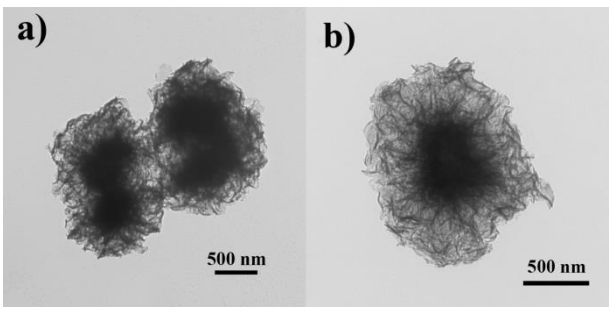

Fig. 2 TEM images of CSH mesoporous microspheres before (a) and after (b) IBU loading.

The STXM images (Figure S1 and S2) are in good agreement with the TEM micrographs: no significant morphology changes are observed from the CSH microspheres before and after IBU loading. Moreover, except for the variations of intensities, which is due to the sample thickness, there are no noticeable spectral differences from different CSH microspheres at Ca $L_{3,2}$-edge, Si K-edge and C K-edge, respectively, indicating the uniformity of CSH microspheres. As a result, we selected individual mesoporous microsphere for a more detailed analysis in the following study.

Figure 3 shows the STXM images of CSH mesoporous microspheres before and after IBU loading taken at the Ca $L_{3,2}$-edge (E = 352.5 eV). The analysis reported below for IBU-loaded CSH mesoporous microspheres is based on the CSH microsphere traced in red dot circle in Figure 3b (STXM analysis of single CSH mesoporous microsphere before IBU loading can be found in Figure S3). Since STXM can provide high quality images as well as high quality absorption spectra at the C K-edge, it has been successfully applied to the studies of carbon nanomaterials.[19, 22, 23] Therefore, it will provide chemical information of the IBU drug molecules from the perspective of the carbon site. Figures 3c to 3e show the STXM images and the C K-edge XANES taken from different regions of interests (ROIs) of an individual CSH microsphere after IBU loading. As shown in Figure 3e, the spectra obtained from different ROIs have identical features. The sharp peak "a" located at 285 eV is from the carbon 1s to π* transition for the aryl rings of IBU molecules; the peak "b" located at 288.3 eV is from the carbon 1s to π* transition for carboxylic functional groups of IBU; the weak peak "c" located around 290 eV is assigned to the transition from carbon 1s to σ* of the C-OH moiety of the carboxylic group.[24-27] Compared with the spectrum of IBU powder (black profile), there is no significant change or beam damage to the IBU molecules, except that peak "c" is less apparent after IBU loading. Based on the STXM and XANES spectra at the C K-edge, it is certain that IBU has been successfully loaded into CSH mesoporous microspheres. We will discuss below in details the chemistry that took place between CSH and IBU during the drug loading process.

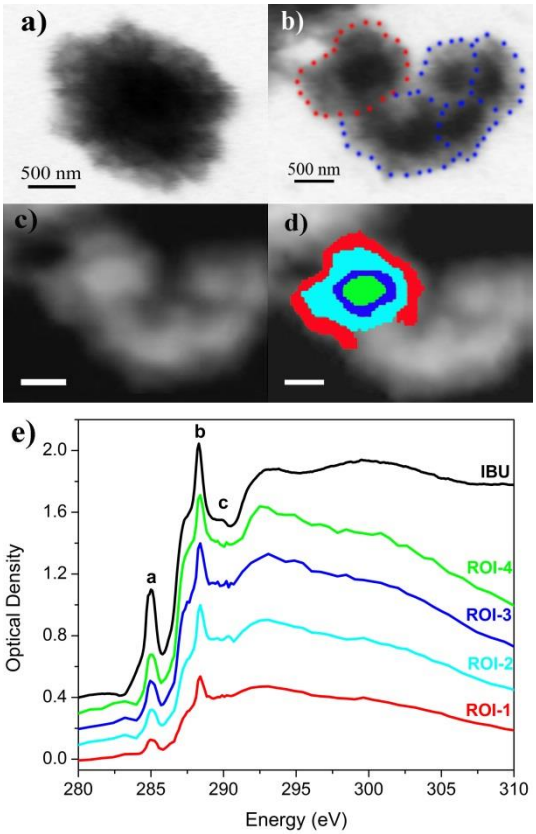

Fig. 3 STXM images of an individual CSH microsphere: (a) before and (b) after IBU loading taken at the Ca $L_{3,2}$-edge (E = 352.5 eV); (c) STXM image of an individual CSH microsphere (average at all edges); (d) 4 ROIs taken from an individual CSH microsphere; Red: ROI-1, Cyan: ROI-2, Blue: ROI-3, Green: ROI-4. Scale bars in (c) and (d) are 500 nm; (e) XANES spectra from each ROI displayed in (d) at the C K-edge.

XANES spectra of the individual CSH microsphere after IBU loading in different ROIs at the Ca $L_{3,2}$-edge, Si K-edge and O K-edge, respectively are shown in Figure 4a, 4b and 4c.

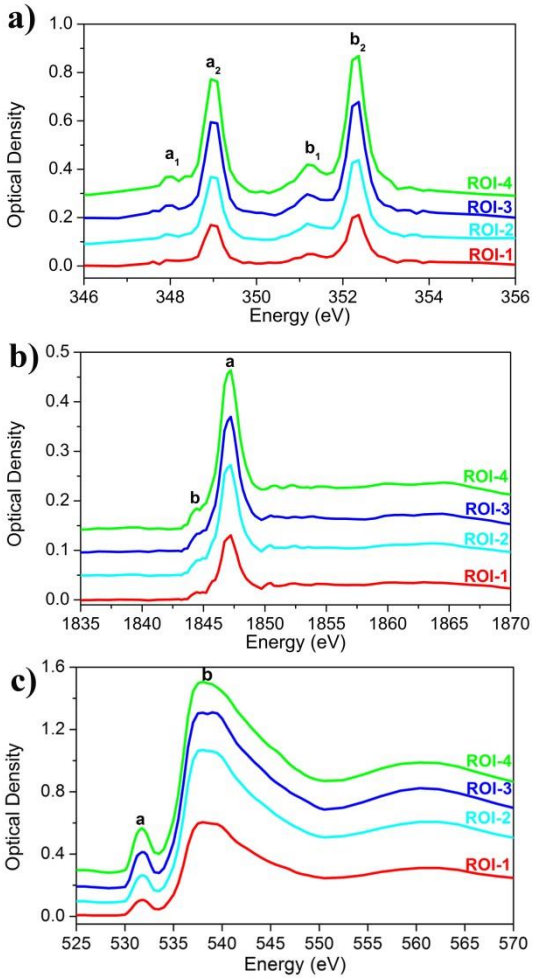

Fig. 4 XANES spectra of individual CSH microsphere after IBU loading at Ca $L_{3,2}$-edge (a), Si K-edge (b) and O K-edge (c). (ROI 1-4 are the same regions as shown in Fig. 3d)

Several interesting features are noticeable. First, at the Ca $L_{3,2}$-edge (Figure 4a), no significant difference in the XANES was observed for different ROIs. The spin-orbit related L_3 (a_2) and L_2 (b_2) peaks before IBU loading (Figure S3), which are located around 349.1 and 352.4 eV respectively, are due to transitions from $2p_{3/2}$ and $2p_{1/2}$ electrons to the empty 3d states of Ca^{2+}. The weak multiple peaks at lower energies are due to crystal field splitting from the first coordination sphere surrounding Ca^{2+}.[28-32] Thus Ca L-edge is sensitive to changes of the magnitude of crystal field and coordination of Ca^{2+}. The Si K-edge XANES spectra are shown in Figure 4b. All spectra show the same features. The main resonance "a" is identified as the Si 1s to 3p transition for silicon (IV) in a tetrahedral oxygen ligand environment.[33, 34] The low energy shoulder "b" is induced by the interaction and will be discussed further. Figure 4c shows the XANES spectra at the O K-edge. There are two discernible features, labelled "a" and "b". The pre-edge peak "a" is due to the Ca–O crystal field effects. The main resonance "b" at around 538 eV is from transition from O 1s to 2p antibonding states hybridized with orbitals of the cations which O is bound. After IBU loading, the XANES spectra of the four ROIs from thin areas (ROI-1 and ROI-2) to thick areas (ROI-3 and ROI-4)) show the same features at all three edges, which means that the CSH microspheres remain chemically uniform after IBU loading. However, having compared the average spectra of CSH microspheres before and after IBU loading at the Ca $L_{3,2}$-edge, O K-edge and Si K-edge, we find discernible changes in the XANES at all edges, as illustrated in Figure 5.

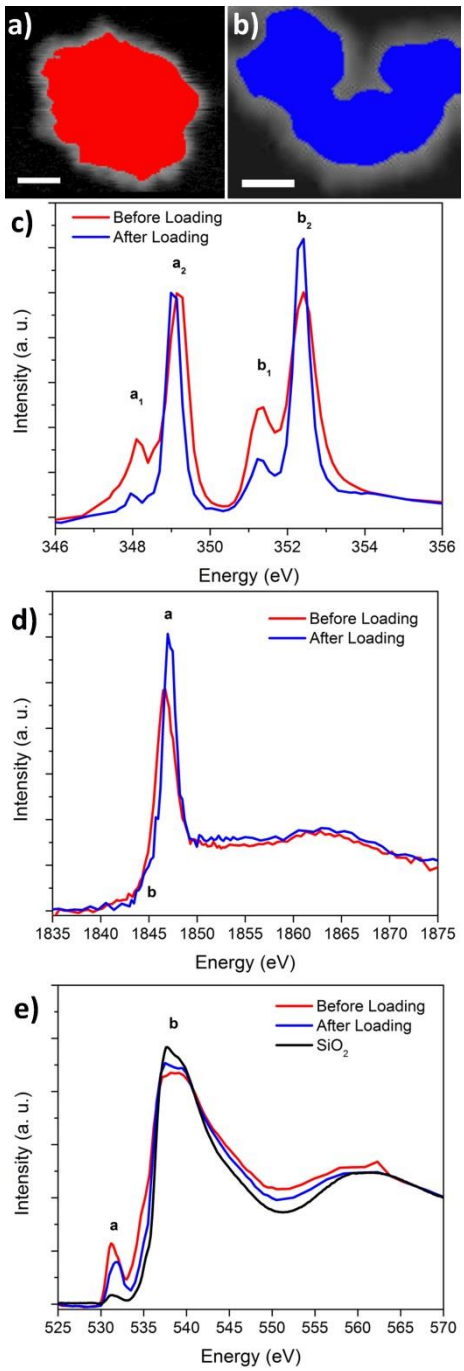

Fig. 5 Comparison of average XANES spectra before (a) and after (b) IBU loading at c) Ca $L_{3,2}$-edge, d) Si K-edge and e) O K-edge.

The presence of Ca-OH groups in CSH has been widely reported in the literature. They are more abundant on the surface or interlayers in order to balance the charge or neutralize the non-bridging oxygens (NBOs).[35-38] In our previous study, we also illustrated that Ca–OH groups located

on the surface or interlayer sites react with the carboxyl groups of IBU directly.[39]

$$\equiv Si\text{-}O\text{-}Ca\text{-}OH + R\text{-}COOH \longrightarrow \equiv Si\text{-}O\text{-}Ca\text{-}O\overset{O}{\overset{\|}{C}}R + H_2O \quad (1)$$

Equation 1. Interaction between CSH and IBU at the Ca local environment.

This interaction between Ca and IBU results in the local environment of Ca is similar to that of calcium acetate after IBU loading. In Figure 5c, there is around 0.1 eV energy shift between the spectra before and after IBU loading. It can be ascribed to the formation of Ca-O-C bonds after IBU loading, which distorts the structure of CSH locally by lowering the symmetry of Ca.[29] The energy differences of ΔL_3 (E_{a2} - E_{a1}), ΔL_2 ($E_{b2} - E_{b1}$) and intensity ratios of a_1 to a_2, b_1 to b_2 of the Ca $L_{3,2}$-edge (see Figure 5c), are listed in Table 1.

Table 1 ΔL_3 and ΔL_2 of CSH microspheres before and after IBU loading*

	ΔL_3 (a_2-a_1) (eV)	$\frac{a_1}{a_2}$	ΔL_2 (b_2-b_1) (eV)	$\frac{b_1}{b_2}$
Before Loading	1.0	0.35	1.0	0.49
After Loading	1.0	0.11	1.1	0.21

* The energy fine step before loading is 0.25 eV and the energy fine step after loading is 0.15 eV

It can be seen that, after IBU loading, there is no significant change in the splitting of a_1 and a_2 (b_1 and b_2 as well). That is because the CSH microsphere we synthesized is composed of $Ca_3Si_2O_7$, which has the crystal structure of rankinite as has been confirmed in previous studies.[20, 35, 40] The calcium atom in CSH is coordinated by seven oxygen atoms while the average coordination number of Ca in calcium acetate is reported to be 7.5.[41-43] While we cannot get much information from the energy differences, the intensity ratio of a_1 to a_2 (as well as b_1/b_2) is informative and it decreases after IBU loading, which indicates that the magnitude of crystal field decreases after IBU loading. Compared to calcium silicate, the crystal field of calcium acetate is weaker because of the difference in ligand electro-negativity.[28, 31] As proposed above, the number of Ca–O–C groups in CSH increases during the IBU loading process, which leads to the decrease of the crystal field (decrease in the intensities of a_1/a_2 and b_1/b_2).

Figure 5d shows the comparison of Si K-edge XANES spectra of the CSH mesoporous microspheres before and after IBU loading. Interestingly, before IBU loading, the main peak "a" is relatively broad; this is due to the differences in chemical environment at Si (IV) sites in the presence of Ca^{2+}. However, after IBU loading, there is a new peak "b" emerges at ~2 eV below the main peak and the main peak became sharper and shifted about 0.5 eV toward higher energy. These observations are in excellent agreement with our previous work (XANES collected on a large area of the specimen).[39] It is proposed that CSH forms some silanol groups (Si-OH) on the surface which interacts with IBU (Equation 2).

$$\equiv Si\text{-}OH + R\text{-}COOH \longrightarrow \equiv Si\text{-}O\text{-}\overset{O}{\overset{\|}{C}}\text{-}R + H_2O \quad (2)$$

Equation 2. Interaction between CSH and IBU at the Si local environment.

In the new structure (Si–O–C), due to the presence of the alkyl groups and the distortion of silicate tetrahedron,[44, 45] we observe that the new peak b is appeared at lower photon energy. On the other hand, most of the Si atoms of calcium silicate in the bulk are still in a SiO_4 tetrahedral environment and after drug loading, most of the silanol groups on the surface could react with the carboxyl groups of IBU. As a result of this interaction, the rest of Si atoms would be in a more "regular" SiO_4 environment leading to that peak "a" turns sharper and shifts to higher energy (the spectra are similar to that of SiO_2 (Figure S4 in supporting information)).

Figure 5e shows the XANES spectra comparison at O K-edge. First, the pre-edge peak "a" shifts from 531.2 eV (due to the Ca–O crystal field effects) to 531.9 eV, which is assigned to the transition from O 1s to π* states (O–C=O, from IBU);[25, 46, 47] Second, the main resonance "b" exhibits splitting into a doublet. When we compare the XANES of CSH loaded with IBU and silicon dioxide (black profile), one can see that the first peak of main resonance of CSH loaded with IBU is similar to that of SiO_2; the Si atoms are in a tetrahedral SiO_4 environment. Based on these observations, we can conclude that the O K-edge XANES spectra of CSH after IBU loading exhibit the chemical characteristics of both CSH and IBU. Besides, the O K-edge results are supplementary to the proposed interactions deduced from the Ca $L_{3,2}$-edge and Si K-edge XANES.

Since STXM can determine the absolute thickness of the sample, thickness distribution maps of the CSH microsphere after IBU loading at Si K-edge and C K-edge can be obtained, as shown in Figure 6a and 6b, respectively.

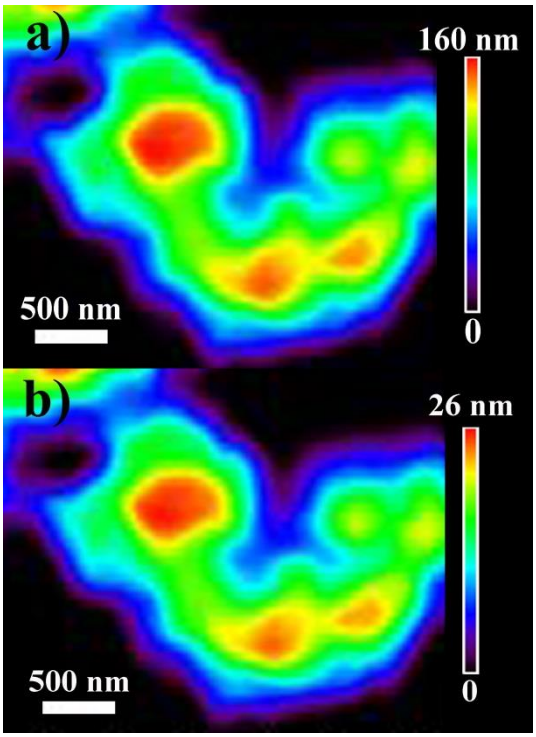

Fig. 6 Thickness distribution maps of an individual CSH microsphere after IBU loading at (a) the Si K-edge and (b) the C K-edge. The vertical bar illustrates the color code of the material thickness.

The thickness was obtained from stack fitting with the quantitatively scaled reference spectra of 1 nm thickness (Figure S5). After drug loading, the material thickness of the centre areas of CSH microsphere is equivalent to ~160 nm (± 10%) of crystalline CSH and that of the surface is around 18 nm (± 10 %) (Figure S6). This thickness of CSH derived from the absorption is smaller than the actual size of the microspheres in TEM (~ 1 μm), which is due to the highly porous structure of the microspheres.[20] Besides, the thickness distribution map of IBU (Figure 6b) is more interesting and significant because the carbon signal is only from IBU molecules and it illustrates the distribution of the drug molecules loaded in the drug carriers (and how much drug molecules can be loaded into the drug carriers by quantitatively comparing the thickness of CSH and IBU). The thickness ratios of CSH to IBU in the thick and thin regions are given in Table 2.

Table 2 Thickness and thickness ratio of CSH to IBU in different regions*

	Thickness (nm)		Ratio
	Si Map	C Map	Si/C
Region 1 (Red)	160	26	6.15
Region 2 (Green)	102	17	6.00
Region 3 (Purple)	18	3	6.00

*There is ± 10% thickness deviation according to Figure 6

IBU were observed on the entire CSH microspheres, and they are more abundant in thick areas (IBU thickness: ~ 26 nm) as compared to the outer surface (IBU thickness is around 2-3 nm); however thickness ratio of Si to C (also representing the thickness ratio of CSH to IBU) remains the same in different regions, which suggests that IBU molecules were uniformly loaded in the mesoporous CSH microspheres.

Conclusions

In summary, we have reported the chemical imaging (with thickness distribution) and interactions between individual CSH microsphere and IBU on an individual meso-microsphere using STXM. Our results suggest that IBU interacts with both Ca-OH and Si-OH groups via its carboxylic acid functional group; this observation confirms previous analysis that based on a large collection of many individual CSH nanostructures in the drug delivery system. We find that the drug loading process has no diverse effect on the integrity of IBU molecules. Moreover, it is of great interest and significance that one can obtain the drug loading distribution in an individual mesoporous CSH microsphere; also, IBU molecules are loaded homogenously into CSH drug carriers.

Acknowledgements

The authors would like to acknowledge Dr. Richard B. Gardiner in Biotron of Western for his assistance in TEM measurement. Research at the University of Western Ontario is supported by NSERC, CRC, CFI, OIT and ASPIRE. The Canadian Light Source is supported by CFI, NSERC, NRC, CHIR, and the University of Saskatchewan. Research at Shanghai Institute of Ceramics is supported by the National Natural Science Foundation of China (51172260, 51302294) and Science and Technology Commission of Shanghai (11nm0506600, 12ZR1452100).

Notes and references

[a] Department of Chemistry, University of Western Ontario, London, Ontario N6A 5B7, Canada.
[b] Shanghai Institute of Ceramics, Chinese Academy of Sciences, Shanghai 200050, China.
[c] Canadian Light Source, Saskatoon, Saskatchewan S7N 2V3, Canada.
‡Equal contribution to this work.
†Electronic Supplementary Information (ESI) available. See DOI: 10.1039/b000000x/

1. A. N. Sawyer, S. Y. Nikonov, A. K. Pancio, L. N. Niu, K. A. Agee, R. J. Loushine, R. N. Weller, D. H. Pashley and F. R. Tay, *J. Endodont.*, 2012, 38, 680-683.
2. Y. D. Dou, C. T. Wu and J. Chang, *Acta Biomater.*, 2012, 8, 4139-4150.
3. J. Wei, F. P. Chen, J. W. Shin, H. Hong, C. L. Dai, J. C. Su and C. S. Liu, *Biomaterials*, 2009, 30, 1080-1088.
4. L. M. Rodriguez-Lorenzo, R. Garcia-Carrodeguas, M. A. Rodriguez, S. De Aza, J. Jimenez, A. Lopez-Bravo, M. Fernandez and J. S. Roman, *J. Biomed. Mater. Res. A*, 2009, 88A, 53-64.
5. C. T. Wu and J. Chang, *Biomed. Mater.*, 2013, 8 032001.
6. D. Arcos and M. Vallet-Regi, *Acta Mater.*, 2013, 61, 890-911.
7. F. Balas, M. Manzano, P. Horcajada and M. Vallet-Regi, *J. Am. Chem. Soc.*, 2006, 128, 8116-8117.
8. M. Vallet-Regi, *Chem. Eur. J.*, 2006, 12, 5934-5943.
9. P. Guttmann, C. Bittencourt, S. Rehbein, P. Umek, X. Ke, G. Van Tendeloo, C. P. Ewels and G. Schneider, *Nature Photonics*, 2012, 6, 25-29.
10. C. Bittencourt, A. P. Hitchock, X. Ke, G. Van Tendeloo, C. P. Ewels and P. Guttmann, *Beilstein J. Nanotechnol.*, 2012, 3, 345-350.
11. E. de Smit, I. Swart, J. F. Creemer, G. H. Hoveling, M. K. Gilles, T. Tyliszczak, P. J. Kooyman, H. W. Zandbergen, C. Morin, B. M. Weckhuysen and F. M. F. de Groot, *Nature*, 2008, 456, 222-U239.
12. A. Felten, C. Bittencourt, J.-J. Pireaux, M. Reichelt, J. Mayer, D. Hernandez-Cruz and A. P. Hitchcock, *Nano. Lett.*, 2007, 7, 2435-2440.
13. B. J. Schultz, C. J. Patridge, V. Lee, C. Jaye, P. S. Lysaght, C. Smith, J. Barnett, D. A. Fischer, D. Prendergast and S. Banerjee, *Nature Commun.*, 2011, 2, 372.
14. Z. Wang, J. Wang, T.-K. Sham and S. Yang, *J. Phys. Chem. C*, 2012, 116, 10375-10381.
15. K. Henzler, P. Guttmann, Y. Lu, F. Polzer, G. Schneider and M. Ballauff, *Nano. Lett.*, 2013, 13, 824-828.
16. T. K. Sham, *Int. J. Nanotechnol.*, 2008, 5, 1194-1246.
17. J. Zhou, X. Zhou, X. Sun, R. Li, M. Murphy, Z. Ding, X. Sun and T.-K. Sham, *Chem .Phys. Lett.*, 2007, 437, 229-232.
18. M. Ushiro, K. Uno, T. Fujikawa, Y. Sato, K. Tohji, F. Watari, W.-J. Chun, Y. Koike and K. Asakura, *Phys. Rev. B*, 2006, 73, 144103.
19. J. Zhou, J. Wang, H. Liu, M. N. Banis, X. Sun and T.-K. Sham, *J. Phys. Chem. Lett.*, 2010, 1, 1709-1713.
20. J. Wu, Y. J. Zhu, S. W. Cao and F. Chen, *Adv. Mater.*, 2010, 22, 749-753.
21. Y. F. Zhu, J. L. Shi, Y. S. Li, H. R. Chen, W. H. Shen and X. P. Dong, *Micropor. Mesopor. Mater.*, 2005, 85, 75-81.
22. J. G. Zhou, J. Wang, C. L. Sun, J. M. Maley, R. Sammynaiken, T. K. Sham and W. F. Pong, *J. Mater. Chem.*, 2011, 21, 14622-14630.
23. J. Zhou, J. Wang, H. Fang, C. Wu, J. N. Cutler and T. K. Sham, *Chem. Commun.*, 2010, 46, 2778-2780.

24. A. Jokic, J. N. Cutler, E. Ponomarenko, G. van der Kamp and D. W. Anderson, *Geochim. Cosmochim. Acta*, 2003, 67, 2585-2597.
25. Y. Zubavichus, A. Shaporenko, M. Grunze and M. Zharnikov, *J. Phys. Chem. A*, 2005, 109, 6998-7000.
26. S. Banerjee, T. Hemraj-Benny, M. Balasubramanian, D. A. Fischer, J. A. Misewich and S. S. Wong, *Chem. Commun*., 2004, 772-773.
27. J. A. Brandes, G. D. Cody, D. Rumble, P. Haberstroh, S. Wirick and Y. Gelinas, *Carbon*, 2008, 46, 1424-1434.
28. F. M. F. de Groot, J. C. Fuggle, B. T. Thole and G. A. Sawatzky, *Phys. Rev. B*, 1990, 42, 5459-5468.
29. F. J. Himpsel, U. O. Karlsson, A. B. Mclean, L. J. Terminello, F. M. F. Degroot, M. Abbate, J. C. Fuggle, J. A. Yarmoff, B. T. Thole and G. A. Sawatzky, *Phys. Rev. B*, 1991, 43, 6899-6907.
30. M. E. Fleet and X. Y. Liu, *Am. Mineral.*, 2009, 94, 1235-1241.
31. S. J. Naftel, T. K. Sham, Y. M. Yiu and B. W. Yates, *J. Synchrotron Radiat.*, 2001, 8, 255-257.
32. J. Ha, S. Chae, K. W. Chou, T. Tyliszczak and P. J. M. Monteiro, *J. Mater. Sci.*, 2012, 47, 976-989.
33. H. Demirkiran, Y. Hu, L. Zuin, N. Appathurai and P. B. Aswath, *Mater. Sci. Eng. C*, 2011, 31, 134-143.
34. D. Li, G. M. Bancroft, M. Kasrai, M. E. Fleet, X. H. Feng, K. H. Tan and B. X. Yang, *Solid State Commun.*, 1993, 87, 613-617.
35. I. Kusachi, C. Henmi, A. Kawahara and K. Henmi, *Mineralogical J.*, 1975, 8, 38-47.
36. A. Nonat, *Cem. Concr. Res.*, 2004, 34, 1521-1528.
37. X. D. Cong and R. J. Kirkpatrick, *Adv. Cem. Based Mater*., 1996, 3, 144-156.
38. J. J. Chen, J. J. Thomas, H. F. W. Taylor and H. M. Jennings, *Cem. Concr. Res.*, 2004, 34, 1499-1519.
39. X. Guo, J. Wu, Y.-M. Yiu, Y. Hu, Y.-J. Zhu and T.-K. Sham, *Phys. Chem. Chem. Phys.*, 2013, 15, 15033-15040.
40. F. J. Qian, R. L. Fu, S. Agathopoulos, X. G. Gu and X. F. Song, *J. Lumin.*, 2012, 132, 71-75.
41. E. A. Klop, A. Schouten, P. Vandersluis and A. L. Spek, *Acta Crystallogr. C*, 1984, 40, 51-53.
42. F. E. Sowrey, L. J. Skipper, D. M. Pickup, K. O. Drake, Z. Lin, M. E. Smith and R. J. Newport, *Phys. Chem. Chem. Phys.*, 2004, 6, 188-192.
43. P. Vandersluis, A. Schouten and A. L. Spek, *Acta Crystallogr. C*, 1987, 43, 1922-1924.
44. Y. F. Hu, R. Boukherroub and T. K. Sham, *J. Electron Spectrosc. Relat. Phenom.*, 2004, 135, 143-147.
45. J. Chaboy, A. Barranco, A. Yanguas-Gil, F. Yubero and A. González-Elipe, *Phys. Rev. B*, 2007, 75, 075205.
46. O. Plekan, V. Feyer, R. Richter, M. Coreno, M. de Simone, K. C. Prince and V. Carravetta, *J. Electron Spectrosc. Relat. Phenom.*, 2007, 155, 47-53.
47. A. Kuznetsova, I. Popova, J. T. Yates, M. J. Bronikowski, C. B. Huffman, J. Liu, R. E. Smalley, H. H. Hwu and J. G. G. Chen, *J. Am. Chem. Soc.*, 2001, 123, 10699-10704.